Polymer Chemistry

RSC Publishing

PAPER

View Article Online
View Journal | View Issue

Cite this: *Polym. Chem.*, 2013, **4**, 3225

An effect on the side chain position of D–π–A-type conjugated polymers with sp^2-hybridized orbitals for organic photovoltaics†

Kwan Wook Song, Ho Jun Song, Tae Ho Lee, Soo Won Heo and Doo Kyung Moon*

Received 6th February 2013
Accepted 9th March 2013

DOI: 10.1039/c3py00195d

www.rsc.org/polymers

A D–π–A-type poly[alkylidenefluorene-*alt*-di-2-thienyl-2,1,3-benzothiadiazole] (**P1**) was synthesized *via* Suzuki coupling reaction. Based on the positions of the spacer (π) and acceptor (A) in the polymers, a dodecyl chain (**P2**) and an octyloxy chain (**P3**), respectively, were introduced. Both chains were introduced to the spacer and acceptor of **P4**. The obtained polymers (**P2–P4**) were soluble in organic solvents such as chlorobenzene, THF and *o*-dichlorobenzene at room temperature. Also, the introduction of a dodecyl chain to the spacer reduced the energy of the highest occupied molecular orbital (HOMO) level (−5.5 to −5.56 eV) but increased the tilt angle (45.4–53.0°), which had prevented the main chain from π–π stacking. The orientation of the obtained polymers in thin films was confirmed by XRD measurement. **P3** with only an octyloxy chain showed a face-on-rich structure with a π–π stacking distance of 3.7 Å compared to other polymers. The polymer solar cells were fabricated through a solution process, and showed a power conversion efficiency (PCE) of 3.6%, with a short-circuit current density (J_{sc}) of 8.9 mA cm^{-2}, an open-circuit voltage (V_{oc}) of 0.88 V, and a fill factor (FF) of 45.7%. With the introduction of poly[9,9-bis(6′-(diethanolamino)hexyl)fluorene] (**PFN-OH**), a PCE of 3.9% was confirmed.

1 Introduction

Organic electronic devices such as organic light-emitting diodes (OLEDs),[1–5] organic photovoltaic cells (OPVs),[6–10] and organic thin-film transistors (OTFTs)[11–14] have been attracting attention owing to their easy manufacturing based on solution processing. As a result, solubility, oxidative stability, and high charge-carrier mobility have been important properties in active materials. Recently, OPVs have been gaining attention as the major research area because of the use of the enhanced molecular engineering technology of π-conjugated polymers. However, the low power conversion efficiency (PCE) of OPVs is a major obstacle. Therefore, in order to enhance the PCE, it is necessary to tune the optoelectronic properties of the photoactive material, *i.e.*, the π-conjugated polymer. Methods of tuning the properties include (1) lowering the energy level of the highest occupied molecular orbital (HOMO) to achieve a high open-circuit voltage (V_{oc}), (2) decreasing the bandgap to enlarge the absorption region, and (3) enhancing the molecular weight of the π-conjugated polymer.[15]

Among the derivatives that lower the HOMO energy levels, the most common are fluorene derivatives.[16,17] These derivatives also have good oxidation stability owing to the low HOMO energy level of fluorene.[18,19] Moreover, because of the introduction of two side chains to the 9-position of fluorene, the poor solubility of π-conjugated polymers can be improved. A method to enlarge the absorption region by decreasing the bandgap involves the introduction of an electron-withdrawing acceptor unit into the main chain of donor–acceptor (D–A)-type polymers. Typical acceptor units that play such a role are 2,1,3-benzothiadiazole (**BT**) and di-2-thienyl-2,1,3-benzothiadiazole (**DTBT**). There have been many studies on the improvement of OPV properties by introducing **DTBT** instead of **BT**. Compared to **BT**, **DTBT** can relieve steric hindrance between a donor and **BT**, thereby increasing the hole mobility. Therefore, the **DTBT** unit has been widely used as the active material in high-efficiency bulk heterojunction (BHJ) polymer solar cells (PSCs).[20,21] However, because of thiophene units in **DTBT**, it has a stronger stacking ability than **BT**. As a result, polymers synthesized with **DTBT** have low solubilities and low molecular weights.[22,23] Therefore, many studies have focused on increasing the molecular weight by using derivatives in which the side chains are introduced to the low-solubility **DTBT**.[23–31] You *et al.* reported the **PBDT–DTBT** series by taking bithiophene fused with a benzene moiety (**BDT**) as a donor and themodified **DTBT** as an acceptor, and the molecular weight and PCE increased over three times by introducing a side chain to the thiophene

Department of Materials Chemistry and Engineering, Konkuk University, 1 Hwayang-dong, Gwangjin-gu, Seoul 143-701, Korea. E-mail: dkmoon@konkuk.ac.kr; Fax: +82-2-444-0765; Tel: +82-2-450-3498

† Electronic supplementary information (ESI) available: ^{1}H NMR spectrum of polymers, cyclic voltammograms of thin films of polymers, a comparison of polymer energy levels using Gaussian calculations, device fabrication and characterization of polymers. See DOI: 10.1039/c3py00195d

spacer.[23] Li *et al.* synthesized D–π–A polymers with a poly(2,7-(9,9′-dioctylfluorene)-*alt*-5,5′-(4,7-di-2-thienyl-2,1,3-benzothiadiazole)) (**F-T-BT-T**) structure. When the side chain was introduced to the thiophene spacer instead of **BT**, a higher increase in molecular weight (over 30 times, to 175 kDa) and a similar PCE (2.2%) were observed. However, the molecular weight of the polymer in which an alkoxy side chain was introduced to **BT** was low (77 kDa), whereas PCE was higher (3.1%) than the former.[27] But, fluorene has two alkyl side chains connected to the C atom with a "sticking-out" configuration. Therefore, even though the substituted alkyl chain improved the solubility of polymers containing fluorene, it is difficult to form a two-dimensional π-stacking morphology, which thus limits close-packing and the charge-carrier mobility.[18,32] McCulloch *et al.* proposed alkylidene fluorene instead of fluorene for close-packing because of the use of the -lidene functional group, which is sp^2-hybridized. This functional group removes the sticking-out effect of the alkyl side chain. Therefore, it has been reported that the alkylidene fluorene homopolymer has a very low intermolecular distance (<0.4 nm) and is available for coplanar conformation. In addition, its HOMO level decreases and an efficient conjugation is enabled along the chain-length.[18] However, this polymer has a wide bandgap (−2.5 eV), which is not sufficient to absorb the solar spectrum.

Recently, Zhang *et al.* performed a study on the close-packing characteristics of polymers. They reported the synthesis of D–π–A-type close-packed polymers by taking **DTBT** as an acceptor and alkylidene fluorene[28] and carbazole,[33] instead of fluorene, as donors. In a separate study, Dai *et al.* concluded that the side chain of the donor polymer in D–π–A-type polymers plays an important role in controlling polymer crystallinity by regulating the main-chain stacking.[32] In particular, **EI-PFDTBT**, to which sp^2-hybridized alkylidene fluorene was introduced, revealed coplanar characteristics. In addition, a device that was spin-coated at 120 °C showed a PCE of 5.07%. However, a low PCE was found (1.53%) in a device that was fabricated at room temperature. Because of the low solubility of polymers, a high-temperature process could be required to form a pinhole- and particle-free uniform and smooth film.[27,28,32]

In this study, D–π–A-type polymers with coplanar conformation, which can be processed at room temperature with high solubility, were synthesized. 9-(1′-Decylundecylidene)fluorene, which has good mobility and oxidative stability with low HOMO levels, was used as an electron donor (D). In addition, alkyl and alkoxy side chains were introduced to the spacer (π) and acceptor (A), respectively, and a poly[alkylidenefluorene-*alt*-di-2-thienyl-2,1,3-benzothiadiazole] (**PAFDTBT**) series was polymerized, as shown in Fig. 1. When the synthesized polymers were fabricated to PSCs at room temperature, a PCE of 3.6% was confirmed. Also, the results revealed a PCE of up to 3.9% by introducing a poly[9,9-bis(6′-(diethanolamino)hexyl)fluorene] (**PFN-OH**) layer. At 480 nm, 60% incident photon-to-current efficiency (IPCE) was demonstrated.

2 Results and discussion

2.1 Polymer synthesis

Scheme 1 shows the general synthetic routes towards both monomers and polymers. In this study, 9-(1′-decylundecylidene)fluorene monomers (D1) were used as the donor and di-2-thienyl-2,1,3-benzothiadiazole (**DTBT**, A1) was used as a strong acceptor. In addition, **DTBT**-adopted dodecyl and octyloxy chains were introduced, depending on the position. As shown in Scheme 1, derivatives with the dodecyl chain (A2) and the octyloxy chain (A3) were introduced to the thiophene spacer and benzothiadiazole, respectively. A4, with both side chains, was also synthesized. Using D1 and **DTBT** derivatives (A1–A4), D–π–A-type polymers (**P1–P4**) were synthesized through a palladium-catalyzed Suzuki coupling reaction (Fig. 1). Polymerization was performed in 2 M aqueous potassium carbonate solution, using toluene as a solvent with $Pd(PPh_3)_4(0)$ as a catalyst and Aliquat 336 as a surfactant at 100 °C for 48 h. Once the polymerization was completed, the samples were end-capped with bromobenzene and phenyl boronic acid. The polymer yields precipitated in methanol (**P1–P4**) were 65, 90, 80 and 80%, respectively. The obtained powders were again purified in a Soxhlet apparatus with methanol, acetone, and chloroform. Finally, the chloroform-soluble portion was re-precipitated in methanol. **P1** was obtained as a dark violet powder, whereas **P2**, **P3** and **P4** were obtained as red powders. The polymers were all well soluble in tetrahydrofuran (THF), chlorobenzene, and *o*-dichlorobenzene at room temperature. The structures of the obtained polymers were confirmed by ^1H NMR spectra (see in ESI†). It was also confirmed that the monomers in which the dodecyl and octyloxy chains were introduced to benzothiadiazole and the thiophene spacer, respectively, were successfully synthesized. Also, according to an analysis of the structure of the obtained polymers, **P2** showed peaks at approximately 2.9–2.6 ppm, which come from the hydrogen bonded to the α-carbon of aromatic thiophene, and **P3** showed peaks at 4.3–4.0 ppm and 2.9–2.6 ppm, which come from the hydrogen bonded to the α-carbon and β-carbon, respectively, of the oxygen in the

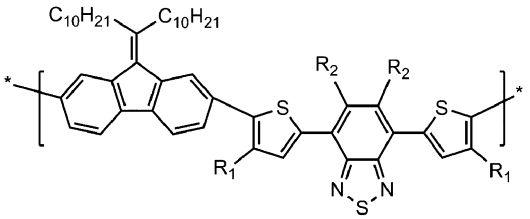

P1 : R_1 = -H, R_2 = -H
P2 : R_1 = -$C_{12}H_{25}$, R_2 = -H
P3 : R_1 = -H, R_2 = -OC_8H_{17}
P4 : R_1 = -$C_{12}H_{25}$, R_2 = -OC_8H_{17}

Fig. 1 Chemical structures of **P1–P4**.

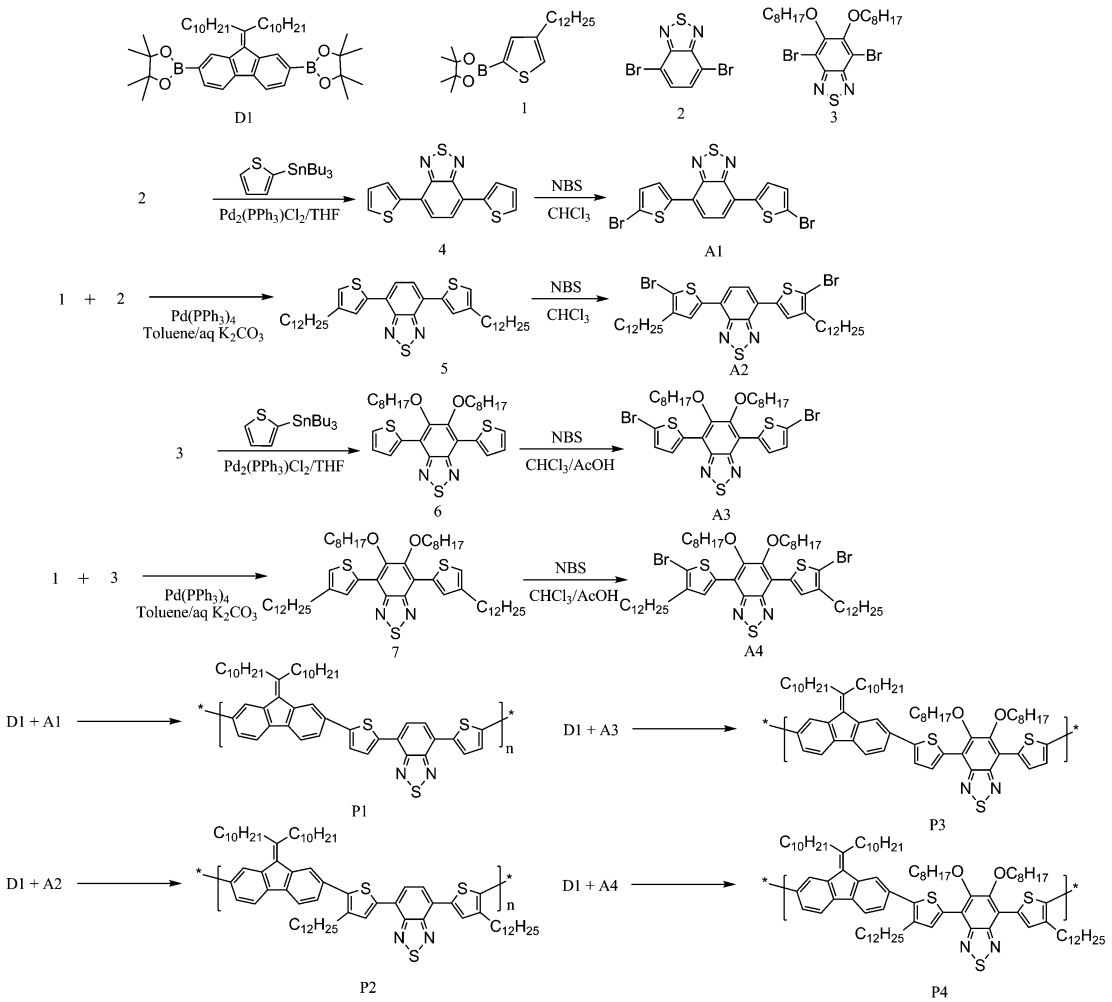

Scheme 1 Synthesis of monomers and polymers.

side chain. In the case of **P4**, aliphatic protons of both **P2** and **P3** were observed.

Table 1 shows the results of the measurement of molecular weights of **P1–P4**. The polymers showed a narrow polydispersity index (PDI) distribution (1.60, 1.54, 2.07, and 1.87) with number-average molecular weights (M_n) of 4.7, 10.1, 17.7, and 8.7 kDa, respectively. **P1** showed a low degree of polymerization with low solubility of the main chain during the polymerization. **P4**, similar to **P1**, also showed a low degree of polymerization despite having both side chains in the thiophene spacer and **BT**. However, in **P2** and **P3**, both M_n and the weight-average molecular weight (M_w) were improved. In particular, **P3** showed the highest degree of polymerization.

These results showed more effectively the increase of molecular weights than those of You *et al.*[23] and Zhang *et al.*[27] You *et al.* reported that polymerization yields and molecular weights were increased regardless of the position of the side chain at the thiophene spacer. In addition, a similar increase in molecular weight was reported when 4-ethyl octyl was introduced at the 5,6-position of **BT**.[23] However, the octyloxy chain introduced to **BT** gave higher molecular weights than the linear dodecyl chain introduced to the thiophene spacer of **DTBT**.

2.2 XRD measurement

Fig. 2 shows the X-ray diffraction measurements of the film to analyze the ordered structure of **P2–P4**. According to a report by Liu *et al.*, a strong diffraction peak was observed at 3.9° and 21.3° in **EI-PFDTBT**, which has a similar structure to **P1**. In addition, the distance between the main chains and the π–π stacking distance were reported to be 22.6 Å and 4.1 Å, respectively.[32] In the out-of-plane of **P2**, a broad diffraction peak was prominently detected at 21.8° which indicates the formation of π–π stacking. According to a calculation based on Bragg's law ($\lambda = 2d\sin\theta$), a

Table 1 Molecular weight of polymers

Polymer	Yield [%]	M_n[a] [kDa]	M_w[a] [kDa]	PDI[a]	Degree of polymerization[b]
P1	65	4.7	7.5	1.60	6
P2	90	10.1	15.6	1.54	9
P3	80	17.7	36.7	2.07	17
P4	80	8.7	16.0	1.87	6

[a] Determined by GPC in tetrahydrofuran (THF) using polystyrene standards. [b] Calculated values which M_n is divided by molecular weight of repeating units.

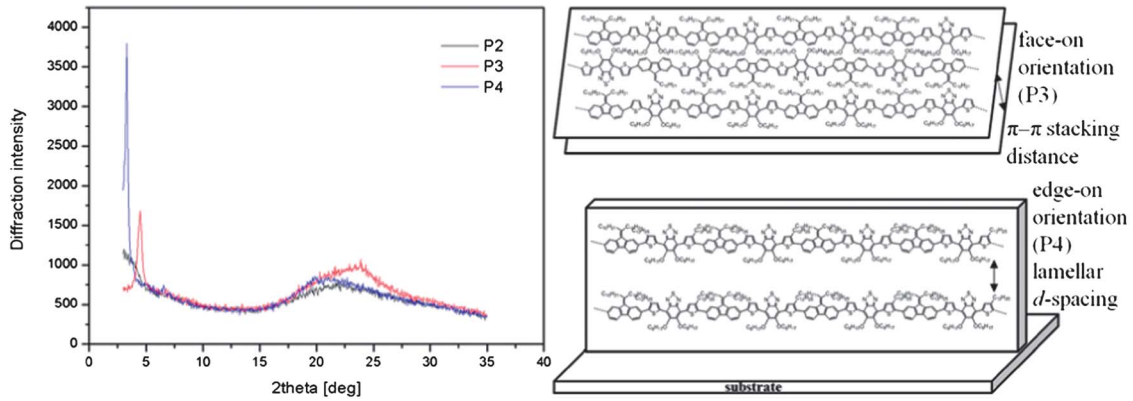

Fig. 2 X-ray diffraction patterns of polymers.

π–π stacking distance (d_π) of 4.1 Å was revealed. The diffraction pattern of **P3** showed a sharp diffraction peak at 4.5°, which indicates the formation of a highly ordered (100) lamellar structure as an out-of-plane peak. The lamellar *d*-spacing (d_1) was calculated to be 19.7 Å. In the (010) crystal plane related to π–π stacking, a broad diffraction peak was observed at 23.8°. The π–π stacking distance (d_π) of **P3** was 3.7 Å. Zhang *et al.* reported that the XRD diffraction peak of **PAFDTBT** is $2\theta = 4.9°$ ($d_1 = 17.9$ Å) and $2\theta = 21.4°$ ($d_\pi = 4.1$ Å). Accordingly, the π–π stacking distance (d_π) of **P3** is smaller than that of **PAFDTBT**.[28] In terms of the diffraction pattern of **P4**, a sharp diffraction peak at 3.3° and a lamellar *d*-spacing (d_1) of 26.6 Å was observed. Moreover, in the (010) crystal plane associated with π–π stacking, a broad diffraction peak was detected at 19.9°, and a π–π stacking distance of 4.5 Å was observed. Therefore, the smallest π–π stacking distance and face-on-rich structure were found in **P3**. And, it can be estimated that an efficient charge transfer would occur in the perpendicular direction. In the case of **P2** and **P4**, because of the dodecyl chain, an amorphous structure was found in **P2**, whereas an edge-on-rich structure was detected in **P4**.

2.3 Optical and electrochemical properties

Fig. 3 shows the UV-visible spectra of all polymers in both solution and film. All polymers were measured at a concentration of 10 μg mL^{-1} in chloroform. All polymers showed two absorption bands. The results are summarized in Table 2. The maximum absorption peak (λ_{max}) of **P1** was 513 nm in solution and the absorption coefficient of **P1** was calculated to be 2.6×10^4 M^{-1} cm^{-1}. In the case of the **P1** film state, the results were red-shifted to 30 nm ($\lambda_{max} = 543$ nm) as compared to the solution. This was due to strong π–π stacking of polymers in the solid state. The absorption edge of **P1** was 675 nm and the calculated optical bandgap was 1.84 eV, which is the lowest among all the synthesized polymers in this study. Therefore, **P1** might undergo absorption in the broadest area of the visible region. In solution, λ_{max} of **P2** was 505 nm. Here, the absorption coefficient was 3.28×10^4 M^{-1} cm^{-1}. As compared to the solution, a 21 nm red-shift ($\lambda_{max} = 526$ nm) was observed in the film. The absorption edge of **P2** was 639 nm, and the calculated optical bandgap was 1.94 eV. Moreover, the **P2** absorption spectra were blue-shifted by 13 nm in solution and by 17 nm in film compared with **P1**. Therefore, anchoring the dodecyl side chain at the 4-position of a thiophene such as in **P2** strengthens the electron donating characteristics. As a result, the absorption coefficient around λ_{max} and the bandgap were increased, whereas π–π stacking tendency is decreased. The UV-visible spectra of **P3** were similar to those of **P1**. **P3** in solution had a λ_{max} of 524 nm, and the absorption coefficient was 3.04×10^4 M^{-1} cm^{-1}. As compared to the **P3**

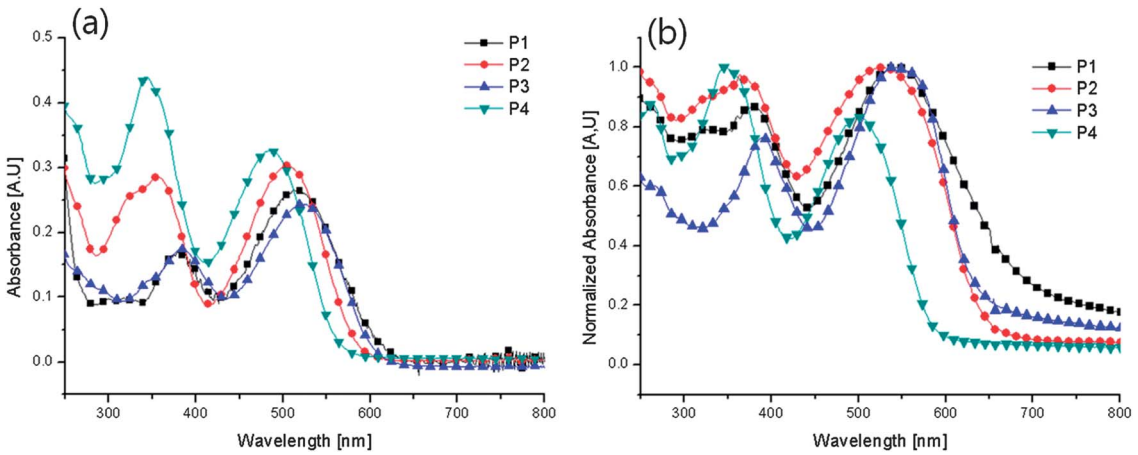

Fig. 3 UV-vis spectra of (a) polymers in chloroform solution at a concentration of 10 μg mL^{-1} and (b) polymers in the film state.

Table 2 Optical and electrochemical data of all polymers

	UV-vis absorption								
	$CHCl_3$ solution		Film			Cyclic voltammetry			DFT
	λ_{max} [nm]	λ_{sh} [nm]	λ_{max} [nm]	λ_{onset} [nm]	E_g^{opa} [eV]	$E_{onset,ox}$ (V)/ HOMO [eV]	$E_{onset,red}$ (V)/ LUMO [eV]	LUMO[b] [eV]	Calcd HOMO [eV]
P1	518	379	543	675	1.84	1.14/−5.41	−0.83/−3.43	−3.57	−4.81
P2	505	355	526	639	1.94	1.29/−5.56	−1.05/−3.22	−3.62	−4.86
P3	524	385	541	643	1.92	1.10/−5.37	−0.85/−3.42	−3.45	−4.74
P4	343	486	346	583	2.12	1.23/−5.50	−1.13/−3.14	−3.38	−4.78

[a] Calculated from the intersection of the tangent on the low energetic edge of the absorption spectrum with the baseline. [b] LUMO = HOMO + E_g^{op}.

solution, a 17 nm red-shift (λ_{max} = 541 nm) was observed in the **P3** film. The absorption edge of **P3** was 643 nm and the calculated optical bandgap was 1.92 eV. These results are similar to the results of the study by Zhang *et al.*[28] By introducing the alkoxy chain, the electron-withdrawing characteristics of the acceptor were weakened and the bandgap of **P3** was increased compared to **P1**. Thus, the alkoxy chains are to make **BT** less electron-accepting. Comparing the UV-visible spectrum behaviours between **P1** and **P3**, it was found that **P3** was more red-shifted in solution, whereas **P1** was more red-shifted in the film. Because the value of the red-shift difference from the solution to the solid state of **P3** (17 nm) is greater than that of **P1** (25 nm), the π–π stacking of **P1** is stronger than that of **P3**. This phenomenon means that film aggregation in **P3** is interrupted by the introduced octyloxy chain. As a result, **P3** has a more unstable chain conformation than **P1**. Finally, λ_{max} of **P4** in solution was 343 nm and the absorption coefficient was calculated to be 5.94×10^4 M^{-1} cm^{-1}, which is greater than the results found for **P1–P3**. In other words, the optical absorption is greater in **P4**. In the solid state a 3 nm red-shift (λ_{max} = 346 nm) was observed compared with that of the solution. The absorption edge of **P4** was 583 nm and the calculated optical bandgap was 2.12 eV. The UV-visible spectra of **P4** were similar to those of **P2**. Here, the electron-donating characteristics and absorption behaviours in the short-wavelength regions were increased because of the dodecyl chain. These results indicate a further increase in the effect of a delocalized π–π* transition.[34] As compared to **P2**, the **P4** spectra in solution were blue-shifted. In addition, the value of red-shift difference from the solution to the solid state was the lowest (3 nm).

Therefore, polymer aggregation was interrupted by the anchored side chains compared to **P1**. Also, the bandgaps of **P2–P4** were increased by the introduced side chains because of decreasing electron-withdrawing characteristics. Especially, when a dodecyl chain is anchored at the spacer, the short wavelength absorption coefficient was enhanced because it gives electron donating characteristics to polymers. Even though all the polymers have the same structure as that of the main chain, the absorption behaviour differed depending on the position of the side chain. The results of the UV-visible spectra were consistent with those of previous studies that were blue-shifted by the introduced side chains to the spacer.[27,29,30,34] However, a study reported by You *et al.* showed a red-shift resulting from the side chain at the 4-position of the spacer compared to that without side chains.[23] Also, a blue-shift resulting from the introduction of a side chain to the **BT** core at the 5,6-position is observed.[23,27] This result is due to chain conformation. But the UV-visible spectra of the **P3** solution in this study were observed to be red-shifted compared to **P1** solution. Therefore, the chain conformation of **P3** is more stable than that of **P1** due to the presence of alkoxy chains.

To check the differences in energy levels as a function of side chains, cyclic voltammograms of the **P1–P4** thin films were measured by using 0.1 M tetrabutylammonium-hexafluorophosphate (**TBAHFP**) in acetonitrile solution, as shown in Fig. S2† and are summarized in Table 2. The dodecyl chain-less **P1** and **P3** showed oxidation onset potentials of +1.14 V and +1.10 V, respectively. The HOMO levels of **P1** and **P3** were similarly calculated to be −5.41 eV and +5.37 eV, respectively. Therefore, we confirmed that the octyloxy chain in **P3** had little effect on the HOMO levels. As reported by Zhang *et al.*, these results were similar to the HOMO level (−5.32 eV) of **PAFDTBT**.[28] However, **P2** and **P4** with dodecyl chains have a greater number of delocalized π electrons. As a result, the oxidation onset potentials of the two polymers were +1.29 V and +1.23 V, respectively. In other words, the deeper HOMO levels of **P2** and **P4** (−5.56 and −5.50 eV, respectively) were calculated as compared to those of **P1** and **P3**. Therefore, the HOMO levels of the polymers decreased because of the increased number of delocalized π-electrons of the alkyl chain. And these results are consistent with the results of previous studies that show reduced HOMO levels, similar to the results of UV-visible spectra.[27,29,30] As compared to **P1** and **P2**, the HOMO levels of **P3** and **P4** slightly increased because of an alkoxy chain which makes **BT** less electron-accepting. This result agrees well with that reported by Zhang *et al.* that the octyloxy chain has a minimal effect in controlling the HOMO levels.[27] Hence, **P2** has the lowest HOMO level, whereas **P3** attains the highest HOMO level. **P4** was influenced by both alkyl and alkoxy chains. However, as reported by You *et al.*, the HOMO levels of polymers were increased by spacers with side chains, whereas those of polymers were decreased by **BT** with side chains.[23]

2.4 Computational study

To have a better understanding of the electronic properties of the synthesized polymers, the molecular geometries and

electron density distribution of states were simulated using density functional theory (DFT). The DFT was calculated using Gaussian 09 for the hybrid B3LYP correlation functional and split valence 6-31G(d) basis set. Oligomers, which have two repeat units, were selected as a calculation model. The calculated HOMO and LUMO orbitals are shown in Fig. 4. The HOMO orbitals were delocalized to the polymer main chain, whereas the LUMO orbitals were localized to the acceptor **BT** because of the structural characteristics of forming quinoid, non-bonding electron pair of nitrogen, and electron-withdrawing characteristics of sulphur.[35] As measured in the cyclic voltammogram, the lowest HOMO level (−4.86 eV) was found in **P2**, whereas the highest HOMO level (−4.74 eV) was found in **P3**. In addition, both were influential in **P4**.

The dihedral angles between the two thienyl groups with central **BT** and alkylidene fluorene were measured. The results are shown in Fig. 4 and are summarized in Table 3. We then attempted to determine the steric hindrance resulting from the introduction of the side chains. In Fig. 4, the dihedral angles **1** of **P1** and **P3** were 24° and 26°, respectively. However, the

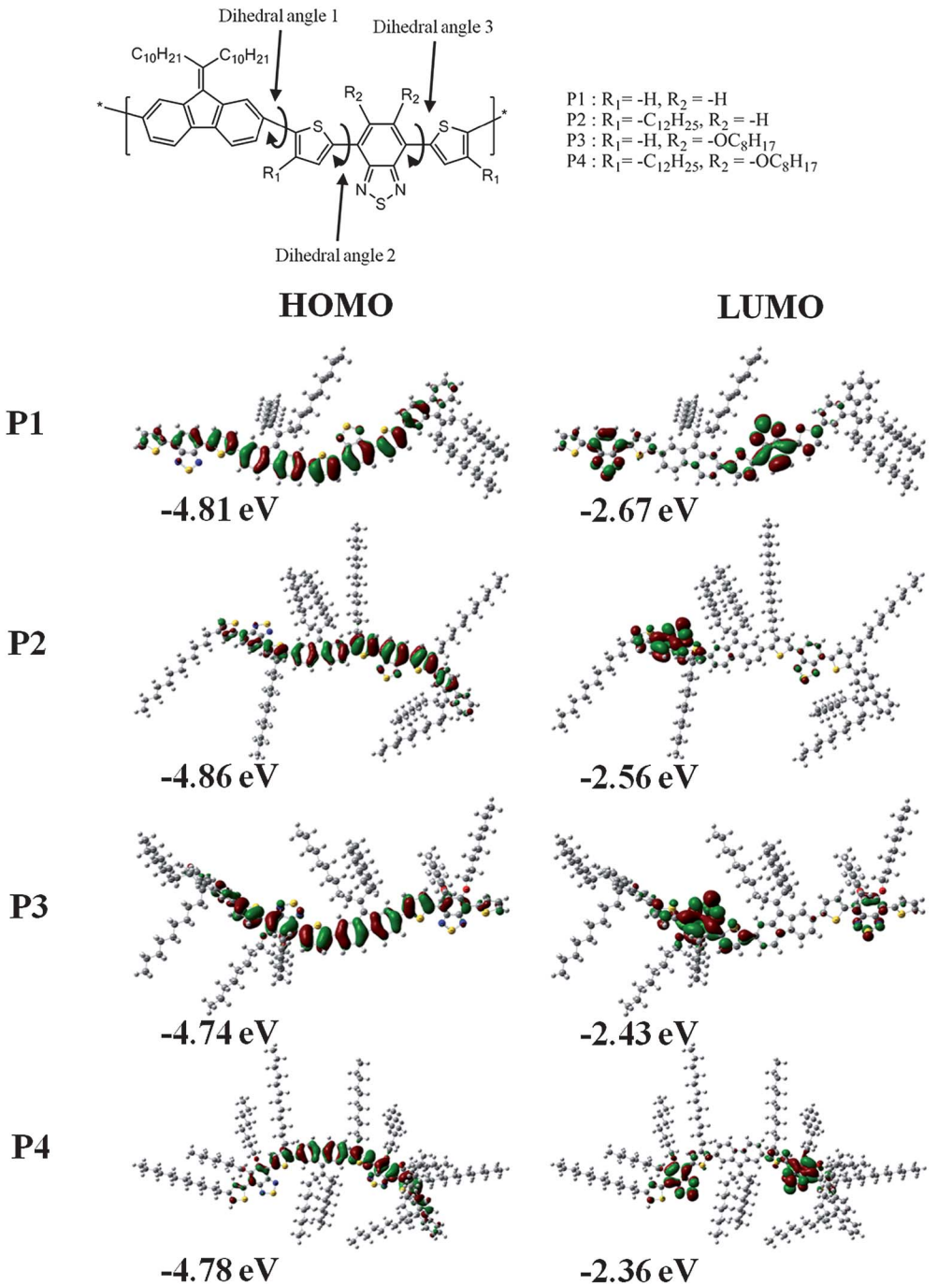

Fig. 4 Calculated HOMO and LUMO orbitals of polymers.

Table 3 Calculated dihedral angles of polymers

Polymers	Dihedral angle 1 (deg)	Dihedral angle 2 (deg)	Dihedral angle 3 (deg)
P1	24.0	5.3	7.8
P2	53.0	17.5	3.5
P3	26.0	17.4	19.8
P4	45.4	16.4	18.7

dihedral angles **1** of **P2** and **P4**, each with thiophene-bound dodecyl side chains, were almost twice those of **P1** and **P3**, at 53° and 45.4°, respectively. Therefore, the alkyl chain at the 4-position is enhancing the steric hindrance. This steric hindrance essentially reduces π–π stacking among the polymers, which can reduce charge transport.[23] **P3** and **P4**, which include alkoxy-chained **BT**, showed an increase in dihedral angles **2** and **3** because of the interaction between oxygen in the alkoxy chain and sulphur in the thiophene spacer.

2.5 Photovoltaic properties

To determine the photovoltaic (PV) properties as a function of the anchoring position of the side chains, BHJ PSCs were fabricated. Fig. 5(a) reveals the *J–V* curve of BHJ PSCs with and without a **PFN-OH** layer in **P3** and **P4**, and Fig. 5(b) shows IPCE. The photovoltaic properties of all polymers were evaluated after fabricating PSC devices with an ITO/PEDOT:PSS/polymer:$PC_{71}BM$/BaF2/Ba/Al structure. All fabricated devices were encapsulated in a glove box. The *J–V* characteristics were measured in an ambient atmosphere with an active area of 4 mm^2. The PV properties of the fabricated PSCs are listed in Table 4. In **P1**, a short-circuit current density (J_{sc}) of 2.7 mA cm^{-2} and a fill factor (FF) of 28.4% were observed with a PCE of 0.55%. Excessive aggregation of **P1** would lead to formation of polymers-only domains so large that excitons cannot reach a donor–acceptor interface.[23] However, the side-chain-anchored polymers, **P2–P4**, showed improved PV properties as compared to **P1**. In addition, **P2** revealed a high V_{oc} of 0.92 V because of a lower HOMO level. However, the increased absorbance was not converted into a photocurrent because **P2** overlapped with the absorption region of the $PC_{71}BM$ acceptor. As a result, the increase in J_{sc} was not significant (J_{sc} = 3.1 mA cm^{-2}). Moreover, because of increased steric hindrance by the alkyl chain, FF somewhat decreased to become 27%. In **P3**, V_{oc} and FF improved despite showing electro-optical properties similar to those of **P1**. In particular, the greatest increase in J_{sc} was found in **P3**, from 2.7 to 8.9 mA cm^{-2}, an increase of 330%. As a result, PCE exhibited an increase of 3.6% because the dissociation of excitons became easier without an energy loss after the series resistance (R_s) reduced. With the other polymers, the greatest V_{oc} was found in **P4** (0.98 V), which had a low PCE of 1.5%. This result of **P4** is because it failed to attain the optimum energy level after an increase in both bandgap and LUMO levels, despite an increase in V_{oc} after the HOMO level became low. As compared to **P2**, the J_{sc} and FF of **P4** improved by 51% and 17%, respectively.

The alcohol/water-soluble polymer **PFN-OH** was introduced to the OPV devices in **P3** and **P4** through the electron-transporting layer.[36,37] **PFN-OH** was melted in methanol (0.05 wt/vol %) and spin-coated on top of the active materials. As a result, V_{oc} and FF in **P3** slightly increased and PCE increased up to 3.9%. Even though V_{oc} decreased in **P4**, J_{sc} increased. In addition, PCE increased up to 1.7% in **P4**.

Consequently, the energy level and steric hindrance changed, depending on the position of the side chain. As a result, in **P2** and **P4**, which have low HOMO levels owing to the dodecyl chain, high V_{oc} values (≥0.9 V) were detected. However, because of the steric hindrance, there was no remarkable

Table 4 Photovoltaic performances of polymers

Polymer	$PC_{70}BM$ ratios	V_{oc} [V]	J_{sc} [mA cm^{-2}]	FF [%]	PCE [%]	R_s [Ω cm^2]
P1	1 : 3	0.72	2.7	28.4	0.55	173
P2	1 : 3	0.92	3.1	27.0	0.78	378
P3	1 : 4	0.88	8.9	45.7	3.6	35.8
P3/PFN-OH	1 : 4	0.93	8.9	47.5	3.9	21.3
P4	1 : 4	0.98	4.7	31.8	1.5	136.8
P4/PFN-OH	1 : 4	0.84	6.2	31.7	1.7	74.2

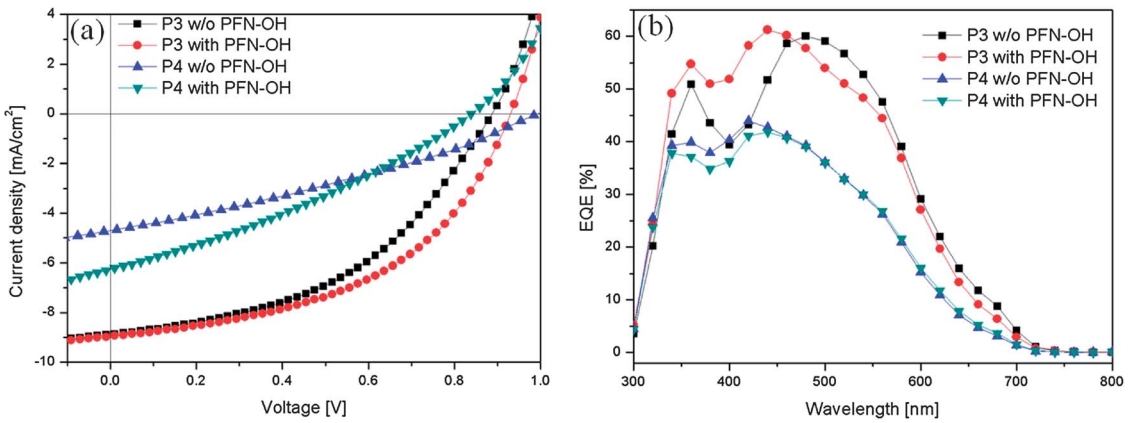

Fig. 5 (a) The *J–V* curve and (b) the IPCE curve of **P3** and **P4** with or without **PFN-OH**.

change in J_{sc} or FF. In **P3**, the lowest R_s was obtained with the introduction of the planar conformation-enabled octyloxy chain.[33] Furthermore, **P3** showed a significant increase in the J_{sc} and FF. Fig. S4(b)† reveals that IPCE of all the polymers exhibited an absorbance of light at 300–700 nm. In particular, **P3**, which revealed the highest J_{sc}, exhibited an IPCE of 60% at 480 nm and a conversion rate of ≥50% with the absorbance of light at 420–520 nm. In the same wavelength region, **P1** and **P2** exhibited an IPCE of 25%, whereas **P4** exhibited an IPCE of 40%.

2.6 Morphology analysis

The morphology of the polymer/$PC_{71}BM$-blend film was measured with atomic force microscopy (AFM) and the results are shown in Fig. 6. The dark-coloured and light-coloured areas correspond to PCBM domains and polymers, respectively. Polymer channels could not be formed in **P1**, **P2**, or **P4**. However, in **P3**, well-defined phase separation between the polymers and $PC_{71}BM$ occurred. In other words, channels were well formed among the polymers. These results are consistent with the high J_{sc} in **P3**. In addition, because the roughness of **P3** is large as compared to **P1** and **P2**, polymer rearrangement occurred. As a result, an ordered structure has become possible, which may be a factor in enhancing the efficiency of PSCs.[38] **P4** has a large root mean square roughness (RMS) of 1.280 nm as compared to the rest of the polymers because of its high steric hindrance.

3 Experimental

3.1 Materials

All starting materials were purchased from Sigma Aldrich and Alfar Aesar, and used without further purification. Toluene and tetrahydrofuran (THF) were distilled from benzophenone ketyl and sodium. 2,7-Bis(4,4,5,5-tetramethyl-1,3,2-dioxaborolan-2-yl)-9-(1-decylundecylidene)fluorene (D1),[7,18] 2-(4-dodecylthiophen-2-yl)-4,4,5,5-tetramethyl-1,3,2-dioxaborolane (**1**),[39] 4,7-dibromo-2,1,3-benzothiadiazole (**2**),[40] 4,7-dibromo-5,6-bis(octyloxy)-2,1,3-benzothiadiazole (**3**),[28] 4,7-di-2-thienyl-2,1,3-benzothiadiazole (**4**), 4,7-bis(5-bromo-2-thienyl)-2,1,3-benzothiadiazole (A1),[41,42] 4,7-bis(4-dodecylthiophen-2-yl)-2,1,3-benzothiadiazole (**5**), 4,7-bis(5-bromo-4-dodecylthiophen-2-yl)-2,1,3-benzothiadiazole

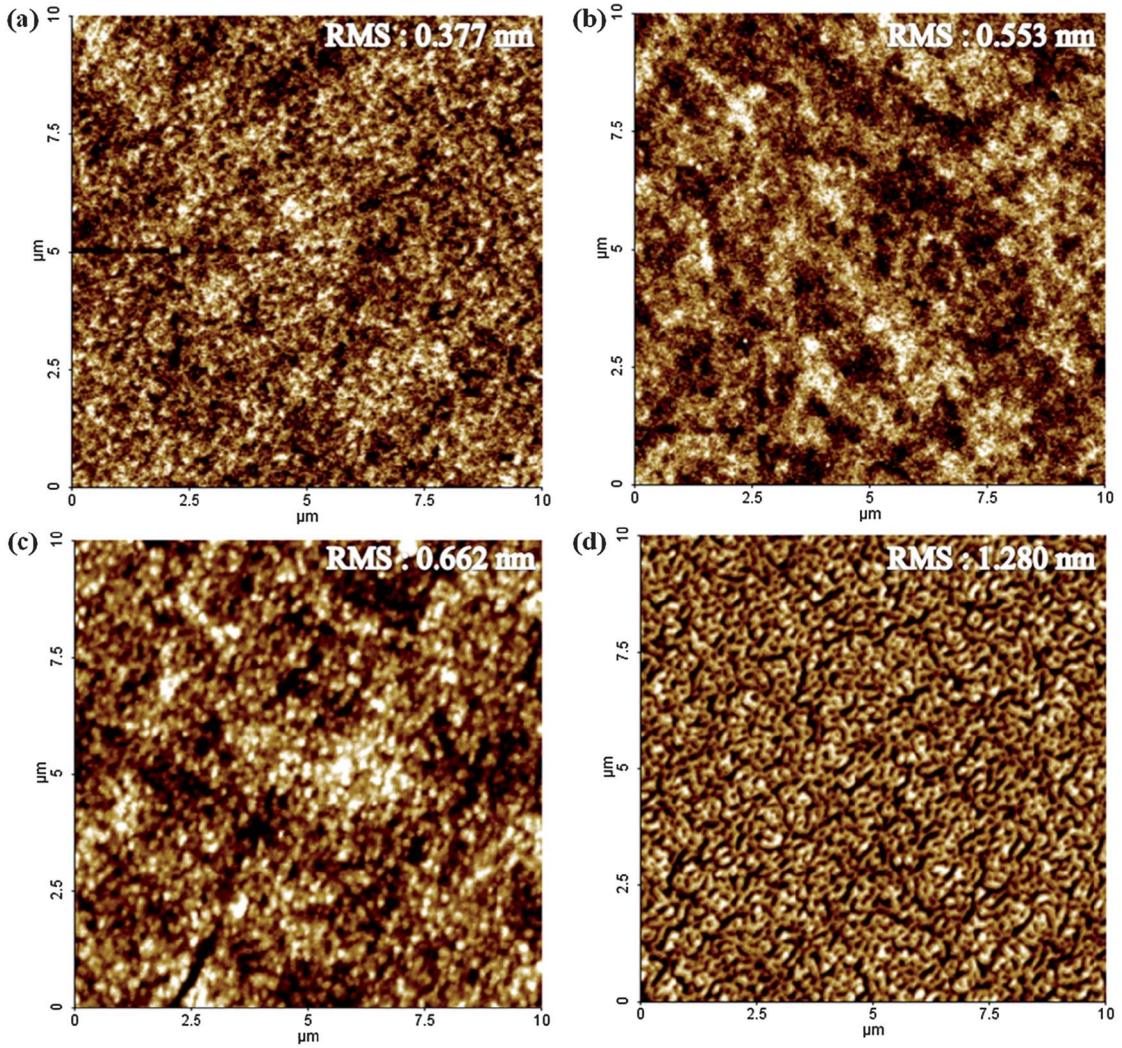

Fig. 6 AFM image (10 × 10 μm^2) of polymers under optimized conditions: (a) **P1**:$PC_{71}BM$ = 1 : 3, (b) **P2**:$PC_{71}BM$ = 1 : 3, (c) **P3**:$PC_{71}BM$ = 1 : 4 and (d) **P4**:$PC_{71}BM$ = 1 : 4.

(A2), 4,7-bis(4-dodecylthiophen-2-yl)-5,6-bis(octyloxy)-2,1,3-benzothiadiazole (**6**), and 4,7-bis(5-bromo-4-dodecylthiophen-2-yl)-2,1,3-benzothiadiazole (A3)[28,43] were prepared according to the literature methods.

3.1.1 4,7-Bis(4-dodecylthiophen-2-yl)-5,6-bis(octyloxy)-2,1,3-benzothiadiazole (7). A mixture of 4,7-dibromo-5,6-bis(octyloxy)-benzo[1,2,5]thiadiazole (1.23 g), 2(4-dodecylthiophene-2-yl)-4,4,5,5-tetramethyl-1,3,2-dioxaborolane (2.2 g), and tetrakis(triphenylphosphine)palladium(0) ($Pd(PPh_3)_4$) (0.13 g, 5 mol%) was dissolved in dry toluene (18 mL) and 2 M K_2CO_3 aqueous solution (3 : 2 in volume). The solution was refluxed for 48 h, then cooled and poured into water. The mixture was extracted twice with chloroform. The organic phases were combined, washed with brine, and dried over anhydrous sodium sulphate. The solvent was removed under reduced pressure and the crude product was purified by column chromatography using chloroform–hexanes as the eluent (ratio 1 : 3) to afford the product as a green powder (0.5 g, 24%). δ_H (400 MHz; $CDCl_3$; Me_4Si): 8.31 (s, 2H); 7.08 (s, 2H); 4.09 (t, 4H, $J = 8$ Hz); 2.71 (t, 2H, $J = 8$ Hz); 1.93 (m, 4H); 1.72 (m, 4H); 1.44–1.32 (m, 60H); 0.88 (t, 6H, $J = 8$ Hz).

3.1.2 4,7-Bis(5-bromo-4-dodecylthiophen-2-yl)-5,6-bis(octyloxy)-2,1,3-benzothiadiazole (A4). 4,7-Bis(4-dodecylthiophen-2-yl)-5,6-bis(octyloxy)-2,1,3-benzothiadiazole (7) (1.3 g) was dissolved into a mixture of acetic acid and chloroform (48 mL) (ratio 1 : 1). Then *N*-bromosuccinimide (0.567 g) was added at 0 °C, and after the addition of NBS, the cooling bath was removed and the reaction was stirred at ambient temperature for 24 h. The solution was then heated up to 55 °C for 24 h. The reaction was carefully monitored by thin layer chromatography (TLC). The reaction mixture was cooled and poured into water. The mixture was extracted three times using chloroform. The chloroform parts were combined, washed with brine, and dried over anhydrous sodium sulphate. The crude product was purified by column chromatography using chloroform–hexanes as the eluent (ratio 1 : 4) to afford the product as a yellow solid (0.5 g, 32%). δ_H (400 MHz; $CDCl_3$; Me_4Si): 8.32 (s, 2H); 4.11 (t, 4H, $J = 8$ Hz); 2.65 (t, 2H, $J = 8$ Hz); 1.94 (m, 4H); 1.67 (m, 4H); 1.46–1.25 (m, 60H); 0.89 (t, 6H, $J = 4$ Hz). Found: C, 61.65; H, 8.24; N, 2.65; O, 3.18; S, 9.19. Calc. for $C_{54}H_{86}Br_2N_2O_2S_3$: C, 61.69; H, 8.25; N, 2.66; O, 3.04; S, 9.15%. MALDI TOF MS: $m/z = 1050.26$ (calculated $m/z = 1050.42$).

3.2 General polymerizations

3.2.1 Representative procedure for polymerization: polymerization of poly[2,2′-(9-(1-decylundecylidene)-9*H*-fluorene-2,7-diyl)-*alt*-4,7-bis(4-dodecylthiophene-2-yl)-5,6-bis(octyloxy)-2,1,3-benzothiadiazole (P4). A mixture of 2,2′-(9-(heptadecan-9-ylidene)-9*H*-fluorene-2,7-diyl)bis(4,4,5,5-tetramethyl-1,3,2-dioxaborolane) (0.196 g), 4,7-bis(5-bromo-4-dodecylthiophene-2-yl)-5,6-bis(octyloxy)-2,1,3-benzothiadiazole (0.290 g) and tetrakis-(triphenylphosphine)palladium(0) ($Pd(PPh_3)_4$) (4 mg, 1 mol%) was dissolved into dry toluene (22 mL) and 2 M K_2CO_3 aqueous solution (3 : 2 in volume). The mixture was vigorously stirred at 80–85 °C for 48 h under nitrogen atmosphere. After the mixture was cooled to room temperature, it was poured into water. The organic mixture was separated and washed with aqueous HCl, ammonium solution and deionized water, respectively. Then, the solvent was removed under the reduced pressure. The organic fraction was precipitated in methanol. The polymer was further purified by washing with methanol and acetone, respectively, in a Soxhlet apparatus for 24 h. The chloroform part was reprecipitated with methanol and then filtered, dried under reduced pressure at 60 °C (0.3 g, 80%).

3.3 Measurements

The ^{1}H NMR (400 MHz) spectra were recorded using a Brüker AMX400 spectrometer in $CDCl_3$, and the chemical shifts were recorded in units of ppm with TMS as the internal standard. Mass spectra were recorded using a Shimadzu Biotech Axima confidence matrix-assisted laser desorption/ionization time-of-flight (MALDI-TOD) mass spectrometer. The elemental analyses were measured with an EA1112 using a CE Instrument. The absorption spectra were recorded using an Agilent 8453 UV-visible spectroscopy system. The solutions that were used for the UV-visible spectroscopy measurements were dissolved in chloroform at a concentration of 10 μg mL^{-1}. The films were drop-coated from the chloroform solution onto a quartz substrate. All of the GPC analyses were carried out using THF as an eluent and a polystyrene standard as the reference. The TGA measurements were performed using a TG 209 F3 thermogravimetric analyzer. The cyclic voltammetric waves were produced using a Zahner IM6eX electrochemical workstation with a 0.1 M acetonitrile (substituted with nitrogen for 20 min) solution containing tetrabutylammonium hexafluorophosphate (Bu_4NPF_6) as the electrolyte at a constant scan rate of 50 mV s^{-1}. ITO, a Pt wire, and silver/silver chloride [Ag in 0.1 M KCl] were used as the working, counter, and reference electrodes, respectively. The electrochemical potential was calibrated against Fc/Fc^+. The HOMO levels of the polymers were determined using the oxidation onset value. Onset potentials are values obtained from the intersection of the two tangents drawn at the rising current and the baseline changing current of the CV curves. The LUMO levels were calculated from the differences between the HOMO energy levels and the optical band-gaps, which were determined using the UV-vis absorption onset values in the films. The current density–voltage (*J*–*V*) curves of the photovoltaic devices were measured using a computer-controlled Keithley 2400 source measurement unit (SMU) that was equipped with a Class A Oriel solar simulator under an illumination of AM 1.5G (100 mW cm^{-2}). Topographic images of the active layers were obtained through atomic force microscopy (AFM) in tapping mode under ambient conditions using an XE-100 instrument.

4 Conclusions

In this study, four polymers were successfully synthesized through Suzuki coupling reaction by anchoring alkoxy and alkyl side chains to alkylidene fluorene (donor) and di-2-thienyl-2,1,3-benzothiadiazole (**DTBT**) derivatives (strong acceptor). The side-chain-less polymer **P1** exhibited the lowest bandgap (1.84 eV) because of aggregation by strong π-stacking, however,

its solubility and molecular weight were low. When side chains were introduced to both the spacer and the acceptor, soluble characteristics and molecular weight increased at room temperature. In **P3**, in which an octyloxy chain was introduced to the acceptor core, the highest molecular weight and face-on-rich structure were attained. In **P4**, which had both alkoxy and alkyl side chains, the strongest steric hindrance and edge-on-rich structure were found. Among the side-chain polymers, a high V_{oc} of 0.88–0.98 V was detected. The highest PCE (3.6%) was observed in **P3**.

Notes

The authors declare no competing financial interest.

Acknowledgements

This research was supported by a grant from the Fundamental R&D Program for Core Technology of Materials funded by the Ministry of Knowledge Economy, Republic of Korea. This work was supported by the National Research Foundation of Korea Grant funded by the Korean Government (MEST) (NRF-2009-C1AAA001-2009-0093526).

References

1 R. H. Friend, R. W. Gymer, A. B. Holmes, J. H. Burroughes, R. N. Marks, C. Taliani, D. D. C. Bradley, D. A. D. Santos, J. L. Bredas, M. Logdlund and W. R. Salaneck, *Nature*, 1999, **397**, 121–128.
2 G. Gustafsson, Y. Cao, G. M. Treacy, F. Klavetter, N. Colaneri and A. J. Heeger, *Nature*, 1992, **357**, 477–479.
3 M. M. Alam and S. A. Jenekhe, *Chem. Mater.*, 2002, **14**, 4775–4780.
4 W. Lu, J. Kuwabara and T. Kanbara, *Macromolecules*, 2011, **44**, 1252–1255.
5 H. J. Song, J. Y. Lee, I. S. Song, D. K. Moon and J. R. Haw, *J. Ind. Eng. Chem.*, 2011, **17**, 352–357.
6 J.-Y. Lee, W.-S. Shin, J.-R. Haw and D.-K. Moon, *J. Mater. Chem.*, 2009, **19**, 4938–4945.
7 J.-Y. Lee, S.-H. Kim, I.-S. Song and D.-K. Moon, *J. Mater. Chem.*, 2011, **21**, 16480–16487.
8 F. C. Krebs, *Sol. Energy Mater. Sol. Cells*, 2009, **93**, 465–475.
9 C. S. Tao, J. Jiang and M. Tao, *Sol. Energy Mater. Sol. Cells*, 2011, **95**, 3176–3180.
10 J. Kuwabara, Y. Nohara, S. J. Choi, Y. Fujinami, W. Lu, K. Yoshimura, J. Oguma, K. Suenobu and T. Kanbara, *Polym. Chem.*, 2013, **4**, 947–953.
11 B.-L. Lee and T. Yamamoto, *Macromolecules*, 1999, **32**, 1375–1382.
12 I. McCulloch, M. Heeney, C. Bailey, K. Genevicius, I. MacDonald, M. Shkunov, D. Sparrowe, S. Tierney, R. Wagner, W. Zhang, M. L. Chabinyc, R. J. Kline, M. D. McGehee and M. F. Toney, *Nat. Mater.*, 2006, **5**, 328–333.
13 T. Yamamoto, H. Kokubo, M. Kobashi and Y. Sakai, *Chem. Mater.*, 2004, **16**, 4616–4618.
14 T. Yasuda, Y. Sakai, S. Aramaki and T. Yamamoto, *Chem. Mater.*, 2005, **17**, 6060–6068.
15 H.-J. Song, D.-H. Kim, E.-J. Lee, S.-W. Heo, J.-Y. Lee and D.-K. Moon, *Macromolecules*, 2012, **45**, 7815–7822.
16 D. F. Perepichka, I. F. Perepichka, H. Meng and F. Wudl, in *Organic Light-Emitting Materials and Devices*, Taylor & Francis Group, 2007, pp. 98–181.
17 D. Jones, in *Organic Photovoltaics*, Wiley-VCH Verlag GmbH & Co. KGaA, 2009, pp. 57–91.
18 M. Heeney, C. Bailey, M. Giles, M. Shkunov, D. Sparrowe, S. Tierney, W. Zhang and I. McCulloch, *Macromolecules*, 2004, **37**, 5250–5256.
19 H. Wang, J. Gao, W. Tong, Q. Qian, K. Lin and F. Liu, *Polym. Chem.*, 2012, **3**, 2794–2800.
20 D.-H. Yun, H.-S. Yoo, S.-W. Heo, H.-J. Song, D.-K. Moon, J.-W. Woo and Y.-S. Park, *J. Ind. Eng. Chem.*, 2013, **19**, 421–426.
21 Y. Zhang, L. Gao, C. He, Q. Sun and Y. Li, *Polym. Chem.*, 2013, **4**, 1474–1481.
22 M. Svensson, F. Zhang, S. C. Veenstra, W. J. H. Verhees, J. C. Hummelen, J. M. Kroon, O. Inganäs and M. R. Andersson, *Adv. Mater.*, 2003, **15**, 988–991.
23 H. Zhou, L. Yang, S. Xiao, S. Liu and W. You, *Macromolecules*, 2010, **43**, 811–820.
24 H. Zhou, L. Yang, S. C. Price, K. J. Knight and W. You, *Angew. Chem., Int. Ed.*, 2010, **49**, 7992–7995.
25 X. Wang, Y. Sun, S. Chen, X. Guo, M. Zhang, X. Li, Y. Li and H. Wang, *Macromolecules*, 2012, **45**, 1208–1216.
26 P. M. Oberhumer, Y.-S. Huang, S. Massip, D. T. James, G. Tu, S. Albert-Seifried, D. Beljonne, J. Cornil, J.-S. Kim, W. T. S. Huck, N. C. Greenham, J. M. Hodgkiss and R. H. Friend, *J. Chem. Phys.*, 2011, **134**, 114901.
27 W. Li, R. Qin, Y. Zhou, M. Andersson, F. Li, C. Zhang, B. Li, Z. Liu, Z. Bo and F. Zhang, *Polymer*, 2010, **51**, 3031–3038.
28 C. Du, C. Li, W. Li, X. Chen, Z. Bo, C. Veit, Z. Ma, U. Wuerfel, H. Zhu, W. Hu and F. Zhang, *Macromolecules*, 2011, **44**, 7617–7624.
29 G. Tu, S. Massip, P. M. Oberhumer, X. He, R. H. Friend, N. C. Greenham and W. T. S. Huck, *J. Mater. Chem.*, 2010, **20**, 9231–9238.
30 S. Song, Y. Jin, S. H. Kim, J. Moon, K. Kim, J. Y. Kim, S. H. Park, K. Lee and H. Suh, *Macromolecules*, 2008, **41**, 7296–7305.
31 Z. B. Lim, B. Xue, S. Bomma, H. Li, S. Sun, Y. M. Lam, W. J. Belcher, P. C. Dastoor and A. C. Grimsdale, *J. Polym. Sci., Part A: Polym. Chem.*, 2011, **49**, 4387–4397.
32 J. Liu, H. Choi, J. Y. Kim, C. Bailey, M. Durstock and L. Dai, *Adv. Mater.*, 2012, **24**, 538–542.
33 R. Qin, W. Li, C. Li, C. Du, C. Veit, H.-F. Schleiermacher, M. Andersson, Z. Bo, Z. Liu, O. Inganas, U. Wuerfel and F. Zhang, *J. Am. Chem. Soc.*, 2009, **131**, 14612–14613.
34 S. Cho, J. H. Seo, S. H. Kim, S. Song, Y. Jin, K. Lee, H. Suh and A. J. Heeger, *Appl. Phys. Lett.*, 2008, **93**, 263301.
35 Z. Ma, E. Wang, M. E. Jarvid, P. Henriksson, O. Inganas, F. Zhang and M. R. Andersson, *J. Mater. Chem.*, 2012, **22**, 2306–2314.

36 F. Huang, Y. H. Niu, Y. Zhang, J. W. Ka, M. S. Liu and A. K. Y. Jen, *Adv. Mater.*, 2007, **19**, 2010–2014.
37 F. Huang, H. Wu and Y. Cao, *Chem. Soc. Rev.*, 2010, **39**, 2500–2521.
38 G. Li, V. Shrotriya, J. Huang, Y. Yao, T. Moriarty, K. Emery and Y. Yang, *Nat. Mater.*, 2005, **4**, 864–868.
39 H. Kong, D. S. Chung, I.-N. Kang, J.-H. Park, M.-J. Park, I. H. Jung, C. E. Park and H.-K. Shim, *J. Mater. Chem.*, 2009, **19**, 3490–3499.
40 R. Yang, R. Tian, J. Yan, Y. Zhang, J. Yang, Q. Hou, W. Yang, C. Zhang and Y. Cao, *Macromolecules*, 2004, **38**, 244–253.
41 Q. Hou, Y. Xu, W. Yang, M. Yuan, J. Peng and Y. Cao, *J. Mater. Chem.*, 2002, **12**, 2887–2892.
42 E. Zhou, S. Yamakawa, Y. Zhang, K. Tajima, C. Yang and K. Hashimoto, *J. Mater. Chem.*, 2009, **19**, 7730–7737.
43 A. Najari, S. Beaupré, P. Berrouard, Y. Zou, J.-R. Pouliot, C. Lepage-Pérusse and M. Leclerc, *Adv. Funct. Mater.*, 2011, **21**, 718–728.